Functional nanostructures of montmorillonite with conducting polyaniline

JONÁŠ TOKARSKÝ[1,2,*], PAVLÍNA PEIKERTOVÁ[1,2],
LENKA KULHÁNKOVÁ[3], KATEŘINA MAMULOVÁ KUTLÁKOVÁ[1],
LUCIE NEUWIRTHOVÁ[1], VLASTIMIL MATĚJKA[1], VÍTĚZSLAV STÝSKALA[4]
AND PAVLA ČAPKOVÁ[5]

[1] *Nanotechnology Centre, VŠB-TU Ostrava, 17. listopadu 15, 708 33 Ostrava, Czech Republic*
[2] *IT4Innovations Centre of Excellence, VŠB-TU Ostrava, 17. listopadu 15, 708 33 Ostrava, Czech Republic*
[3] *Faculty of Metallurgy and Materials Engineering, VŠB-TU Ostrava, 17. listopadu 15, 708 33 Ostrava, Czech Republic*
[4] *Faculty of Electrical Engineering and Computer Science, VŠB-TU Ostrava, 17. listopadu 15, 708 33 Ostrava, Czech Republic*
[5] *Faculty of Science, J.E. Purkyně University, České mládeže 8, 400 96 Ústí nad Labem, Czech Republic*

ABSTRACT: The present work describes the effect of montmorillonite (MMT) particles on the alignment of conducting polyaniline (PANI) chains in a PANI/MMT composite. The composite was prepared both as a powder, pressed into pellets, and as thin films deposited on glass surfaces. For comparison, pure PANI was also prepared in these two forms. A combination of X-ray powder diffraction analysis and molecular modelling confirmed the successful intercalation of the PANI into the MMT, while Raman spectroscopy confirmed the presence of the conducting form of PANI (i.e. the emeraldine salt) in all samples. Scanning electron microscopy, transmission electron microscopy and atomic force microscopy were used to study the morphologies of all samples. Conductivity measurements showed that the presence of the MMT particles in the PANI/MMT composites contributes to a significant increase in the electrical conductivity in comparison with the pure PANI samples. Moreover, in the pressed pellets the presence of the MMT particles led to an extremely high electrical anisotropy. The UV-VIS spectroscopy results showed that the PANI/MMT thin film exhibited a selective transmittance in the range 450–650 nm; therefore, the PANI/MMT thin film is not only conductive, but also suitable for use in various optical applications.

KEYWORDS: polyaniline, montmorillonite, conductivity, structure.

Polyaniline (PANI), a conducting polymer exhibiting good environmental stability and interesting electrical properties, has been studied and used in many different applications (MacDiarmid, 2002). The low cost and wide availability of PANI makes it a useful material for constructing light-emitting diodes (Karg *et al*., 1996), gas sensors (Janata & Josowitz, 2009), pH sensors (Ayad *et al*., 2010) and antistatic coatings (Bhadra *et al*., 2009). Apart from in the powder form, PANI is frequently studied as thin films deposited on various substrates including glass (Stejskal & Sapurina, 2005; Stejskal *et al*., 2010).

The layered structures and unique properties of phyllosilicates are generally a great challenge for the construction of various functional nanostructures. This work is focused on the effect of montmorillonite (MMT) layers on the alignment of conducting PANI chains in the MMT interlayer space (Kulhánková *et al*., 2012; Tokarský *et al*., 2013). The PANI does not form a well-defined crystal structure and self-assembled oligoaniline nanostructures such as PANI nano-tubes, nano-fibres, nano-flakes and nano-ribbons affect their resulting conductivity (Gregory *et al*., 1989; Zujovic *et al*., 2010). In the early stage of crystal order, the self-

assembled nanostructure, which is crucial for the morphology of the PANI samples (Laslau *et al.*, 2012), can be affected by the synthesis pathway (Sapurina & Stejskal, 2008). Ordering of polymer chains can be achieved by various methods, such as mechanical orientation of PANI films (Adams *et al.*, 1996), using blends with insulating polymers (Cao *et al.*, 1993), ordering of the PANI particles in a monomer mixture in an electric field (Stejskal *et al.*, 1997) or by using high pressure (Prokeš *et al.*, 2011). Hybrid PANI/MMT nanocomposites can offer an alternative to such PANI chain ordering as the PANI chains can align along the silicate layers resulting in superior conductivity. The negative silicate layer charge of the MMT helps intercalate the cationic PANI chains into the interlayer space. A series of papers has been published about the preparation and characterization of PANI/MMT nanocomposite powders which achieved a combination of superior electrical and mechanical properties (do Nascimento *et al.*, 2006; Zaarei *et al.*, 2008) and for applications in electrorheology (Lu & Zhao, 2002; Cho *et al.*, 2004) and in the protection of metals from corrosion (Yeh *et al.*, 2001). A recent published work that describes three methods of preparation of PANI/ Ca-MMT nanocomposite powders, focused on the preparation–structure–conductivity relationship and showed a major impact of the preparation process of the PANI/MMT nanocomposites on their conductivity (Kulhánková *et al.*, 2014).

Although powder samples of PANI/MMT nanocomposite have been prepared and characterized extensively in the past, thin film nanocomposites are less common. In this contribution an attempt is made to compare the conductivity of pure PANI and PANI/MMT nanocomposites in the forms of pressed pellets and thin films. The PANI/MMT nanocomposites were investigated using X-ray diffraction (XRD) analysis, Raman spectroscopy, ultra violet-visible (UV-VIS) spectroscopy, electron microscopy, atomic force microscopy (AFM) and molecular modelling and the results were correlated with their DC electrical conductivity.

EXPERIMENTAL

Preparation of the nanocomposites

Aniline, ammonium peroxydisulfate and sulfuric acid were used as received from Lach-Ner (Czech Republic). As a matrix, the Na-montmorillonite, Portaclay® (Ankerpoort NV, Netherlands), was used for the preparation of all composites. The Na-montmorillonite Portaclay® (denoted as MMT) has

the structural formula $Na_{0.7}(Al_{2.85}Mg_{0.71}Ti_{0.02}Fe_{0.42}^{3+})$ $Si_8O_{20}(OH)_4$ with an average layer charge of ~0.7 electrons per unit cell. The d_{001} basal spacing of the MMT is 1.25 nm.

Pure polyaniline (PANI) powder was prepared by *in situ* oxidative polymerization of aniline by mixing equal volumes of two solutions. The first, containing 0.2 M anilinium sulfate in 0.5 M sulfuric acid served as the cation source and the second, containing 0.1 M ammonium peroxydisulfate in distilled water at room temperature, acted as oxidizing agent. After the reaction mixture had turned dark green, as a consequence of the formation of PANI chains, the solid portion was collected on a filter, rinsed with 0.2 M HCl solution to exchange the sulfate ions for chloride ions and the powder dried at 40°C in an oven.

The PANI/MMT nanocomposite powders were prepared in a similar manner using an aqueous suspension of the MMT. However, after the reaction mixture had turned dark green, it was stirred continuously for an additional 6 h to ensure that the PANI chains entered the MMT interlayer space. Subsequently, the green solid was collected on a filter, rinsed with 0.2 M HCl and dried at 40°C. The PANI and PANI/ MMT powders ($m = 3$ g each) were pressed into pellets ($p = 28$ MPa) using a ZWICK 1494 handpress at room temperature without lubrication or binder.

The PANI and PANI/MMT thin films were deposited on a glass surface by the following method. Glass microscope slides were cleaned by washing with a soap solution, rinsed with distilled water, then with ethanol and dried. One side of the glass microscope slides were covered by scotch tape to prevent two-sided coating. The glass slides prepared were attached by clips, hung on strings and introduced into a beaker containing the same reaction mixtures as used for the preparation of the powder samples. After the formation of the PANI or PANI/MMT thin films the glass slides were removed from the beaker, rinsed with 0.2 M HCl and dried at 40°C in an oven. Examples of the pressed pellets and glass slides are shown in Fig. 1.
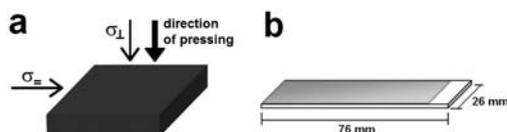

FIG. 1. (a) Pressed pellet with representation of the directions in which the conductivities were measured, i.e. direction of pressing ($\sigma_\perp$) and in the plane ($\sigma_=$) of the pellet; (b) glass slide covered by a thin film.

Characterization methods

X-ray powder diffraction. X-ray diffraction (XRD) measurements of the PANI/MMT nanocomposite powders were carried out in order to confirm the intercalation of the PANI into the MMT and to characterize the degree of preferred orientation of the flat PANI/MMT particles within the nanocomposite pellets. The XRD patterns were recorded with Co$K\alpha$ irradiation ($\lambda = 0.1789$ nm) using a Bruker D8 Advance diffractometer (Bruker AXS) equipped with a VÅNTEC 1 detector.

Transmission and scanning electron microscopy. The morphology of the powder samples was observed with a transmission electron microscope (TEM, JEM-2010, JEOL Ltd.) using a 160 kV accelerating voltage. A LaB$_6$ crystal was used as a source of electrons. The surfaces of the PANI and PANI/MMT thin films were observed on a scanning electron microscope (SEM, Hitachi SU6600 Hitachi Ltd.) at a 20 kV accelerating voltage using the SE (secondary electrons) mode.

Raman spectroscopy. Raman spectra of thin films were measured with a Smart Raman Microscopy System XploRA^{TM} (HORIBA Jobin Yvon, France). The spectra were acquired with a 532 nm excitation laser source, a 50× (powders) or a 100× (thin films) objective, using a 1200 gr./mm grating. The Raman spectra were measured as an evenly-distributed number of points for each sample.

UV-VIS spectroscopy. A UV-VIS Spectrophotometer CINTRA 303 (GBC Scientific Equipment) was used for measurement of optical transmittance spectra of thin films at room temperature. The spectra were measured at normal incidence over the spectral range 300–800 nm. The speed was 1000 nm min^{-1} with a step size of 0.427 nm and a slit width = 2.0 nm. The optical homogeneity of the thin films was investigated using transmittance scanning across the samples. Transmittance measurements were carried out using a Spectrometer Optic Ocean USB2000 + VISNIR instrument equipped with light-collecting large diameter (200 μm) optical fibres. Multi-mode optical fibres were used for precise definition of the measured points. Optical fibres were excited by a halogen light source. Both excitation and collecting fibres (50 μm in diameter) were fixed and the position of the sample was changed by micro sliding.

Atomic force microscopy. The morphology of the surfaces of the thin films was studied using an atomic force microscope (AFM, SolverNEXT, NT-MDT, Russian Federation). A contact probe PPP-CONTR (Nanosensors, Switzerland) was used for imaging and the images were evaluated using the IA P9 software (NT-MDT, Russian Federation).

DC conductivity measurement. Two special devices, constructed for the measurement of electrical conductivity of pressed pellets and thin films, respectively, are shown in Fig. 2. These devices were identical except for the type of contact Cu-electrodes (round and flat for the pellets and linear with a triangular cross-section for the thin films). The DC voltage source (DC POWER SUPPLY HY 3003 D-2) was stabilized to a tolerance of 2.000 ± 10^{-3} V and annexed with an endurance of several tens of seconds to minutes. The electric current passing through the samples was measured over a time interval of 60 s. In the case of pressed pellets the current was measured in two perpendicular directions, i.e. the direction of pressing (denoted as $\sigma_\perp$) and within the plane of the pellet (denoted as $\sigma_=$). The mean value of the electric current was used to calculate the conductivity. An AGILENT 34401A multimeter and a V-meter UNI-T UT802 were used for the calibration. The parameters of measurement were controlled using a computer equipped with a PCI-6221 board. The data obtained were registered and processed using original homemade software prepared in LabVIEW.

Molecular modelling. The Materials Studio modelling environment was used to study the interlayer arrangement in PANI/MMT nanocomposites. Structure data published by Tsipursky & Drits (1984) and Méring & Oberlin (1967) were used to build the MMT crystal structure under periodic boundary conditions as a 6a × 3b × 1c supercell with the crystallochemical formula $(Al_{46}Mg_{16}Fe_{10}^{3+})Si_{144}O_{360}(OH)_{72}$. The total negative layer charge x = –16 el., arising from octahedral substitutions, was compensated by Na$^+$ cations and/or PANI chains prepared as dimers having charge x = 4 el., placed in the MMT interlayer space. Initial models with different Na$^+$/PANI ratios (16/0, 12/1, 8/2, 4/3, 0/4) containing various amount of H$_2$O molecules were prepared and optimized using the Materials Studio/ Forcite module. The atoms in the models were parameterized by using the Universal force field method (Rappé *et al.*, 1992). The basal spacings of the optimized models were calculated using the Materials Studio/Reflex module with the experimental conditions: Bragg-Brentano geometry; $\lambda(CoK\alpha) =$
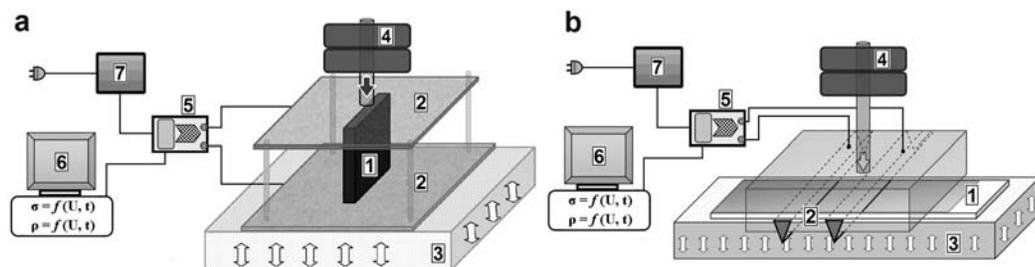
FIG. 2. Experimental apparatus for measuring the DC conductivity of (a) pellets and (b) thin films. (1) sample (pellet or thin film); (2) Cu electrodes; (3) flexible insulator; (4) weights to ensure a constant load; (5) measuring card; (6) PC + software; (7) DC voltage source.

0.1789 nm; $2\theta = 5–50°$ and the results compared with d_{001} values obtained from real samples in order to find the most probable interlayer arrangement.

RESULTS AND DISCUSSION

PANI and PANI/MMT pressed pellets

The XRD traces for the original MMT and the PANI/MMT composite are shown in Fig. 3. The original MMT exhibits a large 001 profile broadening suggesting an inhomogeneous interlayer structure. The shift of the 001 reflection towards lower °2θ suggests that in the PANI/MMT composite, the PANI chains had intercalated the MMT. The diffraction profile of the PANI/MMT intercalate is sharper, suggesting a more homogeneous interlayer structure. This conclusion was supported by molecular modelling results that show good agreement of d_{001} values calculated from simulated diffraction patterns of optimized models with the d_{001} values obtained experimentally. The best agreement was achieved for the PANI/MMT models that contained two flat-laying PANI chains in a monolayer arrangement with eight Na^+ cations and ~4.4 wt.% of H_2O in the MMT interlayer space (Figs. 4a, b). The basal spacings calculated from the models with various positions of the Na^+ cations and H_2O molecules ($d_{001} = 1.277–1.296$ nm), correspond to the real sample of the PANI/MMT powder having a d_{001} spacing = 1.28 nm (Fig. 3). The PANI/MMT composite pressed into pellet gave a d_{001} spacing = 1.33 nm (Fig. 3), which corresponds to the $d_{001} = 1.321–1.368$ nm obtained from simulated XRD patterns of optimized models containing three PANI chains, four Na^+ cations and ~1.5 wt.% of H_2O molecules in the MMT interlayer space (Fig. 4c, d). The PANI chains in these models were also arranged in a monolayer, but the aromatic rings were tilted. Note

that these models represent the arrangement of the interlayer species corresponding to the greatest-intensity 001 reflections. Taking into account the width of the 001 reflections, other interlayer arrangements can also be expected and it is also probable that un-intercalated domains are also present in the PANI/MMT sample.

Comparison of the 001 reflections (Fig. 3) revealed that intercalation had a positive influence on the ordering of the MMT layers. While the basal reflection of the MMT exhibits significant broadening, the basal reflections of the PANI/MMT powder and the PANI/MMT
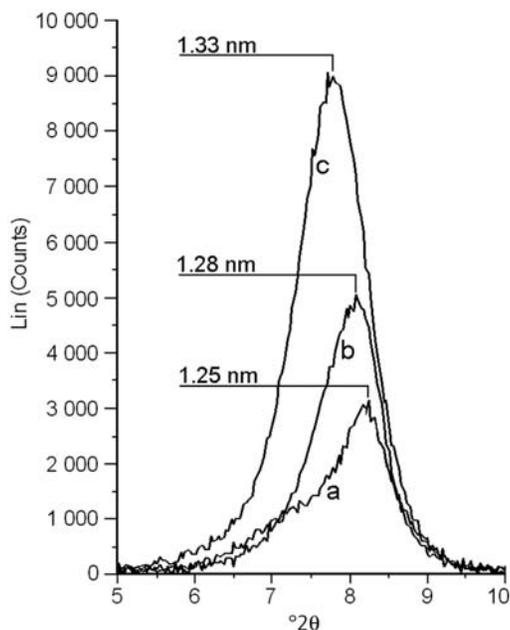

FIG. 3. XRD profiles of 001 basal reflection: (a) for the original MMT powder; (b) for the PANI/MMT powder; and (c) for the PANI/MMT pressed pellet.
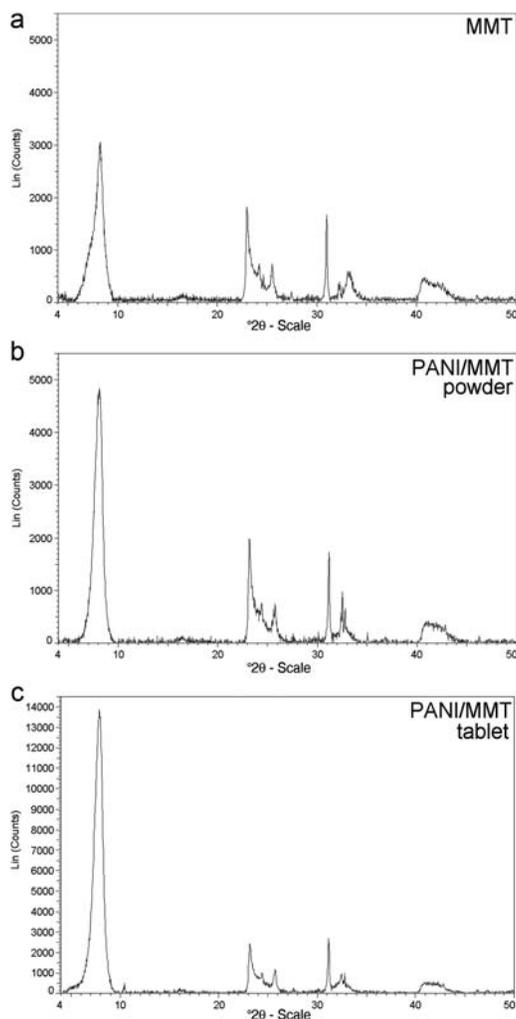
FIG. 4. Full diffraction patterns (range 4–50°2θ) of the MMT powder, the PANI/MMT powder and the PANI/MMT pressed pellet.

TABLE 1. In-plane conductivity ($\sigma_=$) and orthogonal conductivity measured in the direction of pressing ($\sigma_\perp$) for the PANI and PANI/MMT pellets. Anisotropy factor $\alpha = \sigma_= / \sigma_\perp$.

Samples	Conductivity σ [S/m]		Anisotropy Factor, α
	$\sigma_\perp$	$\sigma_=$	
PANI	1.04	6.94	6.7
PANI/MMT	0.01	8.40	1016

4–50°2θ) of the MMT powder, the PANI/MMT powder and the PANI/MMT pressed pellet are shown in Fig. 4.

The electrical conductivities of the PANI and PANI/MMT pellets measured in the direction parallel to the main surface of the pellet ($\sigma_=$) and in the direction of pressing ($\sigma_\perp$) are listed in Table 1, together with values of the anisotropy factor, α, calculated as the ratio: $\sigma_= / \sigma_\perp$. This factor describes the tendency towards two-dimensional conductivity.

The PANI/MMT pellet exhibits a very high anisotropy factor as a consequence of the strong texture mentioned above. The $\sigma_\perp$ value is low because the MMT layers that are arranged parallel to the main surface of the pellet serve as insulators. On the other hand, the more regular arrangement of the PANI chains inside the MMT structure and along the MMT layers results in greater $\sigma_=$ conductivity than in the case of pure PANI. The low, but still observable, electrical anisotropy of pellets pressed from the PANI powder is not surprising when the elongated shape of the PANI grains (see Fig. 6a) is considered. It can be expected that such elongated grains have a tendency to arrange parallel to one another under external pressure and, therefore, will also form a textured structure, which is reflected in the electrical properties.

The MMT particles in the PANI/MMT composite are coated with PANI, which is less rod-shaped than in pure PANI (Fig. 6b). This is demonstrated in the greater resolution of the image (Fig. 6c) where the smaller and rounder PANI grains can be seen clearly in the upper right corner (compare Figs 6a and 6c).

The Raman spectra of the PANI and PANI/MMT powders are shown in Figs 7a and 7b. The spectrum of the pure MMT matrix is not shown, as no bands were detected due to the fluorescence of the clay mineral (Frost & Rintoul, 1996). Thus, the spectra show the typical PANI spectrum with all its characteristic bands and only the most significant

pressed pellet are sharper indicating a more homogeneous interlayer structure due to the arrangement of the PANI chains. The d_{001} spacing of the MMT in the pressed pellet is larger than that of the MMT in the powder. This increase during pressing can be explained by additional intercalation of the MMT by PANI and/or by preferential ordering of the MMT particles, both of which enhance the intensity of the 001 reflection. Figure 3 also shows the strong texture of the pressed pellet clearly (see the increase in the 001 reflection intensity), i.e. due to the MMT (001) planes becoming oriented perpendicular to the direction of pressure. Full diffraction patterns (range
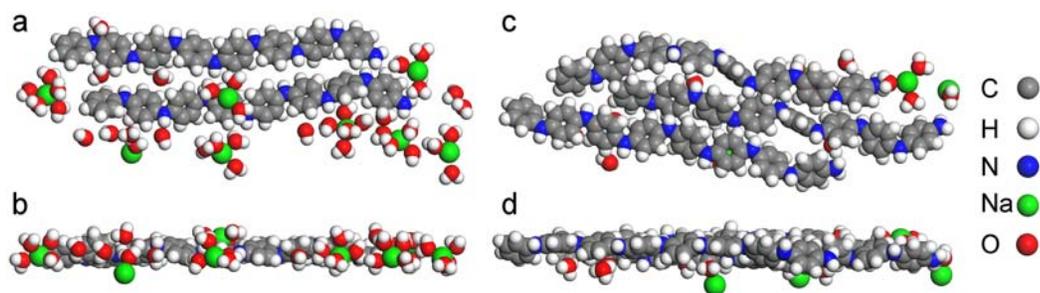
FIG. 5. Optimized models of the PANI/MMT interlayer content showing the interlayer arrangement in the PANI/MMT powder – view along the [001] direction (a); view along the [100] direction (b); and in the PANI/MMT pressed pellet – view along the [001] direction (c); view along the [100] direction (d).

bands of the PANI are described in this study. A detailed description of these characteristic bands can be found in Tokarský *et al.* (2014). The broad band at higher wavenumbers (above 2000 cm^{-1}) is typical for the conducting form of PANI (Epstein *et al.*, 1987). The presence of the conducting PANI (emeraldine salt) was also proven by the most important band located at 1342 cm^{-1} corresponding to the $C–N^{+\bullet}$ bond (da Silva *et al.*, 1999). This so-called "protonation band" characterizing the protonation state of the PANI is more intense in the PANI spectrum than in the PANI/MMT spectrum (compare Figs 7a and 7b). Nevertheless, the greater conductivity of the PANI/MMT sample (Table 1) suggests that not only the protonation state of the PANI, but also the different structural ordering of the PANI in the presence of MMT, affect the conductivity of the composite. The presence of quinonic units in the PANI/MMT (Fig. 7b) was revealed by the band at 1643 cm^{-1} (Šeděnková *et al.*, 2008), which is absent

from the spectrum of the pure PANI powder (Fig. 7a). However, the bands located at 584 and 1402 cm^{-1}, assigned to phenoxazine and phenazine-type units (do Nascimento *et al.*, 2002, 2004), can be found in both samples. These units match with the cross-linked parts of the PANI structure. Their interpretation is still not definitive, but it is known that the molecular structure containing these units is more stable (do Nascimento *et al.*, 2008).

PANI and PANI/MMT thin films

The morphology of the PANI and PANI/MMT thin films, observed using AFM, are shown in Fig. 8. The effect of the presence of the MMT particles is evident on the resulting morphology of the surface of the PANI/MMT nano-composite thin film. By comparing the surface of the pure PANI (Fig. 8a) and PANI/MMT thin films (Fig. 8b) the uniform arrangement of MMT particles is clearly visible, while the pure PANI forms
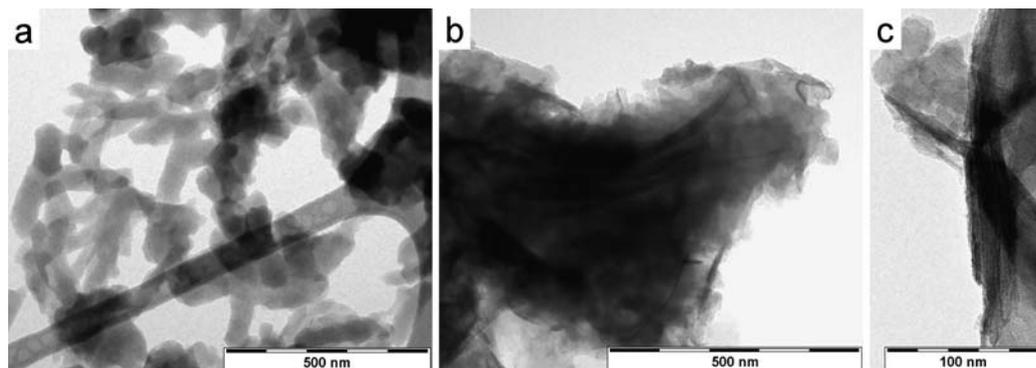

FIG. 6. (a) TEM image of the PANI powder; the sample is composed of rod-shaped grains ∼200 nm long and diameter of ∼50 nm. (b) and (c) Covering of the MMT particles (dark elongated bodies) by PANI in the composite.
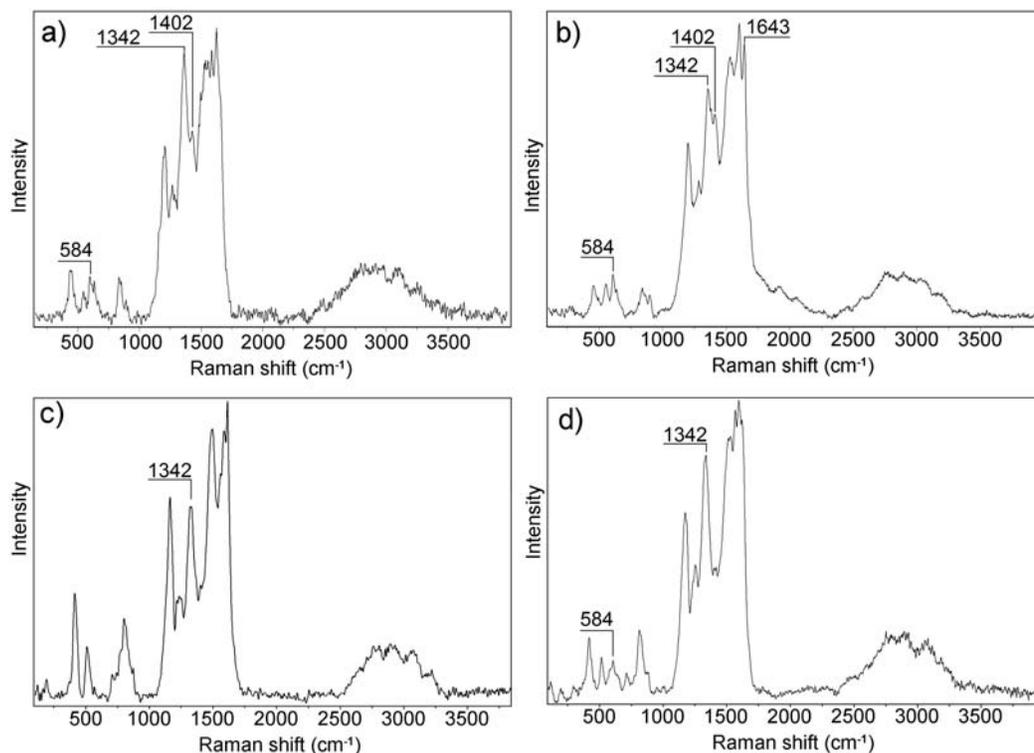
FIG. 7. Raman spectra: (a) of the PANI powder; (b) of the PANI/MMT powder; (c) of the PANI thin film; and (d) of the PANI/MMT thin film.

humps and prickles sticking out of the film. The thicknesses of the films were also determined using AFM. A streak, perpendicular to the surface of thin film, was made with a razor blade (see the smooth regions in the right part of Fig. 8a, b) and, subsequently, the height of this "step" was measured. The heights of both films are listed in Table 2. The thickness of the PANI/MMT film is 2.7 times greater than that of the PANI film and the electrical conductivity is four times greater (Table 2), thus showing the influence of the MMT particles on the conductivity.

The maximum transmittance was 520 nm for both the PANI and PANI/MMT thin films (Fig. 9). The transmittance of the PANI/MMT thin film is much less than for the pure PANI film (Table 2), but the PANI/MMT is more optically homogeneous. The transmittance homogeneity $\Delta T = T_{max} - T_{min}$ has been determined as the difference between the maximum and minimum transmittance detected across the sample at $\lambda = 520$ nm. Transmittance maps for the pure PANI and PANI/MMT films are compared in Fig. 10.

The Raman spectra of the PANI and PANI/MMT thin films are similar to the Raman spectra of the PANI and PANI/MMT powders (compare Fig. 7a,b and 7c,d) indicating that the conducting PANI form (emeraldine salt) was also obtained in the PANI and PANI/MMT

TABLE 2. Conductivity (σ), thickness (t), wavelength range of transmitted light (λ), transmittance homogeneity (ΔT) and the integral value of the transmittance measured over the entire surface of the sample (T_{int}).

Samples	σ [S/m]	t [nm]	λ [nm]	ΔT (520 nm) [%]	T_{int} (520 nm) [%]
PANI	90	138	(*)	10	75
PANI/MMT	356	375	450–650	6	8

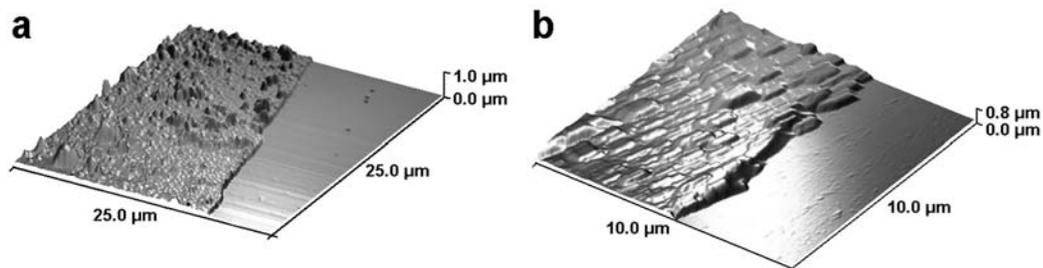(*) transparent over the whole range measured.

F<small>IG</small>. 8. AFM images (a) of the PANI and (b) of the PANI/MMT thin films.

thin films. The high intensity of the protonation band (1342 cm^{-1}) may result from the treatment of the thin films with HCl to remove the sulfate ions. The difference between the Raman spectra of the powders and films is due to the lack of bands corresponding to the phenoxazine and phenazine-type units. In the spectrum of the PANI thin film the bands at 584 and 1402 cm^{-1} are absent and only the band at 584 cm^{-1} is visible in the spectrum of the PANI/MMT thin film (Fig. 7d). Hence, the PANI thin film is more conductive than the PANI in powder form (compare Tables 1 and 2), but is probably less stable. However, the spectra of the PANI/MMT samples (powder and film) show more bands of the cross-linking units than their counterparts without MMT and thus the samples with MMT are probably more stable.

One of the most interesting results was obtained by measurement and comparison of the optical transmittances (Table 2, Fig. 9). The PANI thin film is transparent in the 300–800 nm range of wav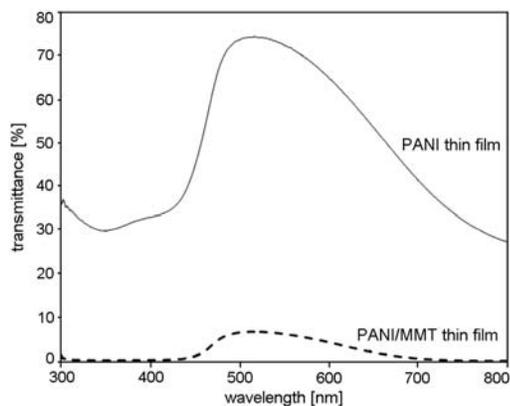elengths, while the PANI/MMT film is transparent only in the range 450–650 nm. This can be useful in applications where selective transmittance is required. The fact that the PANI/MMT films are still transparent can be explained by the ability of MMT to form transparent layers (Ogawa & Kuroda, 1995). However, it must also be noted that although the position of maximum transmittance ($\lambda = 520$ nm) remained the same for both samples, the maximum transmittance itself decreased by >9× for the PANI/MMT thin film (see Table 2). However, the comparison of the transmittance homogeneity shows that the PANI/MMT thin film is less permeable, but more optically homogenous (Fig. 10).

The SEM images and EDX spectra of thin films are shown in Fig. 10. The pure PANI film (Fig. 11a) is covered by small PANI aggregates, formed in the polymerization solution and adhering to the surface of the PANI film. The source of silicon in point 1 (Fig. 11a) is the glass substrate, while for point 2 (Fig. 11b) the MMT particles are the source of the silicon. Point 3 was placed in an area of the PANI/MMT film with no MMT particles in order to compare the EDX spectrum with that of the pure PANI film. The lower silicon content at point 3 in comparison with point 1 in the pure PANI film is due to the greater thickness of the PANI/MMT film (see Table 2). Figure 11c shows a larger area of the PANI/MMT film and an even distribution of MMT particles. The sulfur and chlorine in the EDX spectra come from the ammonium peroxydisulfate, sulfuric acid and hydrochloric acid used for the preparation of the samples.

CONCLUSIONS

A PANI/MMT composite was prepared both in powder form and as a thin layer deposited on a glass surface, using a simple one-step process. Raman spectroscopy confirmed the presence of the protonated form of PANI in all samples prepared. The layer structure and charge of the MMT affect the arrangement of the PANI chains
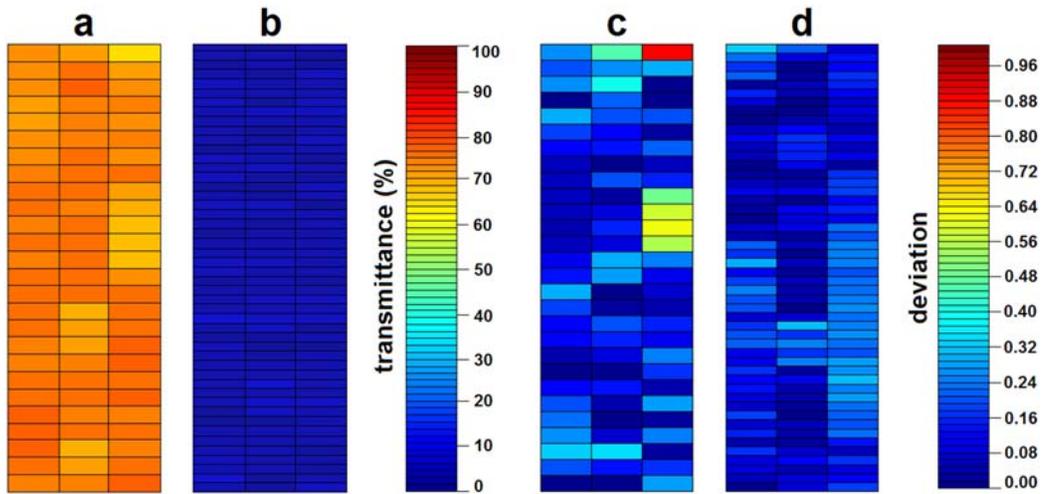

F<small>IG</small>. 9. Transmittance spectra of the PANI and PANI/MMT thin films deposited on glass substrate.

FIG. 10. Transmittance mapping across (a) the PANI and (b) the PANI/MMT thin films for wavelength λ = 520 nm, with deviations from the average values (c) for the PANI and (d) the PANI/MMT thin films. It is evident that rough surface of the pure PANI films is less homogeneous than the smooth surface of the PANI/MMT thin film.
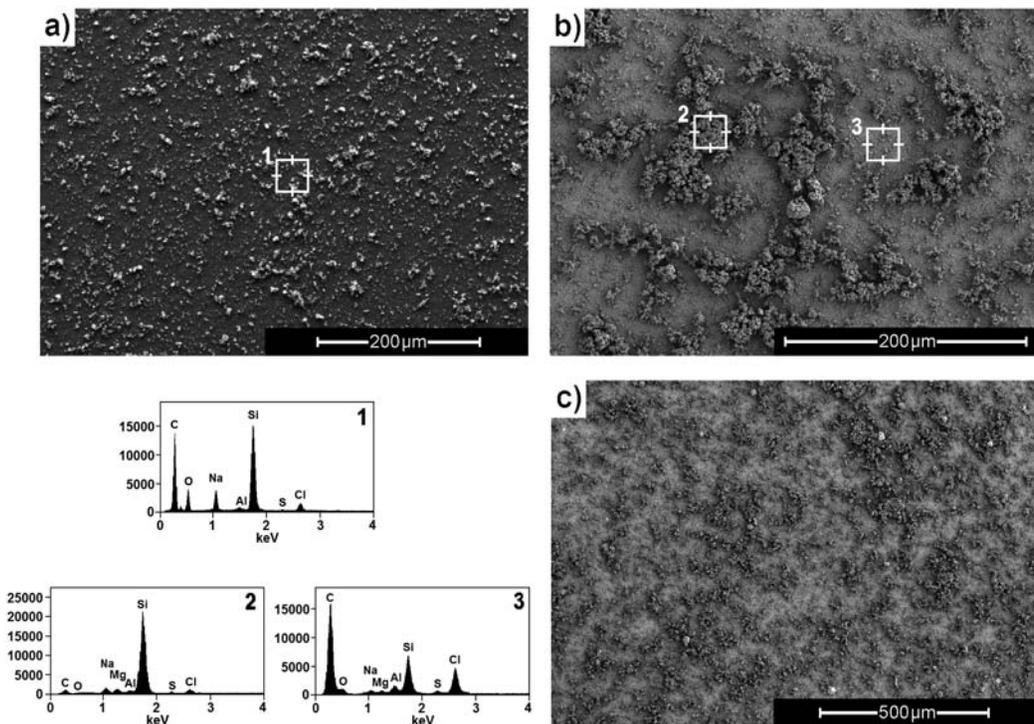

FIG. 11. SEM images (a–c) and EDX spectra at points 1–3 indicated on the PANI thin film (a, 1) and PANI/MMT thin film (b, 2 & 3 and c).

in the PANI/MMT composite positively, as suggested by the increase in electrical conductivity of both pressed pellets and thin films. In the pellets, the platy MMT particles are arranged perpendicular to the direction of pressure. When measuring the conductivity in the direction of pressure, the MMT layers prevent the flow of electrical current, thus leading to a greater electrical anisotropy of the pressed pellets.

In the case of thin layers one could expect that the PANI chains are arranged on the glass surface more regularly than in either the powder or pellet forms. This assumption was confirmed by comparison of the conductivities of the pellets and layers. Most importantly, the high conductivity of the PANI thin films can be increased still further by the presence of the MMT particles and conductivity values >350 S/m might be reached.

Taking into account the in-plane conductivities only of the pressed pellets, the increases in the in-plane conductivity of the samples can be summarized as follows: PANI pellet (6.9 S/m) < PANI/MMT pellet (8.4 S/m) < PANI thin film (90 S/m) < PANI/MMT thin film (356 S/m). Using the average conductivity calculated from both directions, the values change slightly, but the order remains the same: PANI pellet (3.99 S/m) < PANI/MMT pellet (4.2 S/m) < PANI thin film (90 S/m) < PANI/MMT thin film (356 S/m). These observations confirm the expected positive effect of the negatively charged silicate layers on the alignment of the PANI chains. This effect results not only in a significant increase in the electrical conductivity, but also in better optical homogeneity of the PANI/MMT thin films. The increase in electrical conductivity of the PANI/MMT thin films is accompanied by a decrease in the optical transparency.

ACKNOWLEDGMENTS

REFERENCES

Adams P.N., Laughlin P.J. & Monkman A.P. (1996) Synthesis of high molecular weight polyaniline at low temperatures. *Synthetic Metals*, **76**, 157–160.

Ayad M.M., Salahuddin N.A., Algaysh M.O. & Issa R.M. (2010) Phosphoric acid and pH sensors based on polyaniline films. *Current Applied Physics*, **10**, 235–240.

Bhadra S., Khastgir D., Singha N.K. & Lee J.H. (2009) Progress in preparation, processing and applications of polyaniline. *Progress in Polymer Science*, **34**, 783–810.

Cao Y., Smith P. & Heeger A.J. (1993) Counter-ion induced processibility of conducting polyaniline, *Synthetic Metals*, **57**, 3514–3519.

Cho M.S., Choi H.J. & Ahn W.S. (2004) Enhanced electrorheology of conducting polyaniline confined in MCM-41 channels. *Langmuir*, **20**, 202–207.

Epstein A.J., Ginder J.M., Zuo F., Bigelow R., Woo H.S., Tanner D.B., Richter A.F., Huan W.S. & MacDiarmid A.G. (1987) Insulator-to-metal transition in polyaniline. *Synthetic Metals*, **18**, 303–309.

Frost L.R. & Rintoul L. (1996) Lattice vibrations of montmorillonite: an FT Raman and X-ray diffraction study. *Applied Clay Science*, **11**, 171–183.

Gregory R.V., Kimbrell W.C. & Kuhn H.H. (1989) Conductive textiles. *Synthetic Metals*, **28**, 823–835.

Janata J. & Josowitz M. (2009) Organic semiconductors in potentiometric gas sensors. *Journal of Solid State Electrochemistry*, **13**, 41–49.

Karg S., Scott J.C., Salem J.R. & Angelopoulos M. (1996) Increased brightness and lifetime of polymer light-emitting diodes with polyaniline anodes. *Synthetic Metals*, **80**, 111–117.

Kulhánková, L., Tokarský, J., Peikertová, P., Mamulová Kutláková, K., Ivánek L. & Čapková, P. (2012) Montmorillonite intercalated by conducting polyanilines. *Journal of Physics and Chemistry of Solids*, **73**, 1530–1533.

Kulhánková, L., Tokarský, J., Peikertová, P., Ivánek L., Mamulová Kutláková, K. & Čapková, P. (2014) Conductivity of polyaniline/montmorillonite nanocomposites prepared under various conditions. *Materials Technology – Advanced Performance Materials*, **29**, 301–306.

Laslau C., Ingham B., Zujovic Z.D., Čapková, P., Stejskal J., Trchová, M. & Travas-Sejdic J. (2012) Synchrotron X-ray scattering reveals early-stage crystallinity during the self-assembly of polyaniline nanotubes with rectangular cross-sections. *Synthetic Metals*, **161**, 2739–2742.

Lu J. & Zhao X.P. (2002) Electrorheological properties of a polyaniline–montmorillonite clay nanocomposite suspension. *Journal of Materials Chemistry*, **12**, 2603–2605.

MacDiarmid A.G. (2002) Synthetic metals: a novel role for organic polymers. *Synthetic Metals*, **125**, 11–22.

Méring J. & Oberlin A. (1967) Electron-optical study of smectites. *Clays and Clay Minerals*, **27**, 3–25.

do Nascimento G.M., Constantino V.R.L. & Temperini M.L.A. (2002) Spectroscopic characterization of a

new type of conducting polymer-clay composite. *Macromolecules*, **35**, 7535–7537.

do Nascimento G.M., Constantino V.R.L., Landers R. & Temperini M.L.A. (2004) Aniline polymerization into montmorillonite clay: a spectroscopic investigation of the intercalated conducting polymer. *Macromolecules*, **37**, 9373–9385.

do Nascimento G.M., Constantino V.R.L., Landers R. & Temperini M.L.A. (2006) Spectroscopic characterization of polyaniline formed in the presence of montmorillonite clay. *Polymer*, **47**, 6131–6139.

do Nascimento G.M., Silva C.H.B., Izumi C.M.S. & Temperini M.L.A. (2008) The role of cross-linking structures to the formation of one-dimensional nano-organized polyaniline and their Raman fingerprint. *Spectrochimica Acta Part A*, **71**, 869–875.

Ogawa M. & Kuroda K. (1995) Photofunctions of intercalation compounds. *Chemical Reviews*, **95**, 399–438.

Prokeš J., Varga M., Křivka I., Rudajevová A. & Stejskal J. (2011) The influence of compression pressure on transport properties of polyaniline. *Journal of Materials Chemistry*, **21**, 5038–5045.

Rappé A.K., Casewit C.J., Colwell K.S., Goddard W.A. & Skiff W.M. (1992) UFF, a full periodic table force field for molecular mechanics and molecular dynamics simulations. *Journal of the American Chemical Society*, **114**, 10024–10035.

Sapurina I. & Stejskal J. (2008) The mechanism of the oxidative polymerization of aniline and the formation of supramolecular polyaniline structures. *Polymer International*, **57**, 1295–1325.

da Silva J.E.P., de Tiorresi S.I.C., de Faria D.L.A. & Temperini M.L.A. (1999) Raman characterization of polyaniline induced conformational changes. *Synthetic Metals*, **101**, 834–835.

Stejskal J., Špírková M., Quadrat O. & Kratochvíl P. (1997) Electrically anisotropic materials: polyaniline particles organized in a polyurethane network. *Polymer International*, **44**, 283–287.

Stejskal J. (2002) Polyaniline. Preparation of a conducting polymer (IUPAC Technical Report). *Pure and Applied Chemistry*, **74**, 857–867.

Stejskal J. & Sapurina I. (2005) Polyaniline, thin films and colloidal dispersions (IUPAC Technical Report). *Pure and Applied Chemistry*, **77**, 815–826.

Stejskal J., Sapurina I. & Trchová, M. (2010) Polyaniline nanostructures and the role of aniline oligomers in their formation. *Progress in Polymer Science*, **35**, 1420–1481.

Šeděnková I., Trchová M. & Stejskal J. (2008) Thermal degradation of polyaniline films prepared in solutions of strong and weak acids in water – FTIR and Raman spectroscopic studies. *Polymer Degradation and Stability*, **93**, 2147–2157.

Tokarský J., Stýskala V., Kulhánková L., Mamulová Kutláková K., Neuwirthová L., Matějka V. & Čapková P. (2013) High electrical anisotropy in hydrochloric acid doped polyaniline/phyllosilicate nanocomposites; effect of phyllosilicate matrix, synthesis pathway and pressure. *Applied Clay Science*, **80–81**, 126–132.

Tokarský J., Maixner M., Peikertová P., Kulhánková L. & Burda J.V. (2014) The IR and Raman spectra of polyaniline adsorbed on the glass surface; comparison of experimental, empirical force field, and quantum chemical results. *European Polymer Journal*, **57**, 47–57.

Tsipurski S.I. & Drits V.A. (1984) The distribution of octahedral cations in the 2:1 layers of dioctahedral smectites studied by oblique-texture electron diffraction. *Clay Minerals*, **19**, 177–193.

Yeh J.M., Liou S.J., Lai C.Y. & Wu P.C. (2001) Enhancement of corrosion protection effect in polyaniline via the formation of polyaniline–clay nanocomposite materials. *Chemistry of Materials*, **13**, 1131–1136.

Zaarei D., Sarabi A.A., Sharif F. & Kassiriha S.M. (2008) Structure, properties and corrosion resistivity of polymeric nanocomposite coatings based on layered silicates. *Journal of Coating Technology and Research*, **5**, 241–249.

Zujovic Z.D., Laslau C., Bowmaker G.A., Kilmartin P.A., Webber A.L., Brown S.P. & Travas-Sejdic J. (2010) Role of aniline oligomeric nanosheets in the formation of polyaniline nanotubes. *Macromolecules*, **43**, 662–670.